Brief communication: CESM2 climate forcing (1950-2014) yields realistic Greenland ice sheet surface mass balance

Brice Noël[1], Leonardus van Kampenhout[1], Willem Jan van de Berg[1], Jan T. M. Lenaerts[2], Bert Wouters[1,3], and Michiel R. van den Broeke[1]

[1]Institute for Marine and Atmospheric research (IMAU), Utrecht University, Utrecht, Netherlands
[2]Department of Atmospheric and Oceanic Sciences, University of Colorado Boulder, Boulder CO, USA
[3]Department of Geoscience and Remote Sensing, Delft University of Technology, Delft, Netherlands

Correspondence: Brice Noël (b.p.y.noel@uu.nl)

Abstract.

We present a reconstruction of historical (1950-2014) surface mass balance (SMB) of the Greenland ice sheet (GrIS) using a high-resolution regional climate model (RACMO2; ∼11 km) to dynamically downscale the climate of the Community Earth System Model version 2 (CESM2; ∼111 km). After further statistical downscaling to 1 km spatial resolution, evaluation using in situ SMB measurements and remotely sensed GrIS mass change shows good agreement, including the recently observed acceleration in surface mass loss (2003-2014). Comparison with an ensemble of eight previously conducted RACMO2 simulations forced by climate reanalysis demonstrates that the current product accurately reproduces the long term average and variability of individual SMB components, and captures the recent increase in meltwater runoff that accelerated GrIS mass loss. This means that, for the first time, climate forcing from an Earth System Model (CESM2), that assimilates no observations, can be used without additional corrections to reconstruct historical GrIS SMB and the mass loss acceleration that started in the 1990s. This paves the way for attribution studies of future GrIS mass loss projections and contribution to sea level rise.

1 Introduction

A common approach to project the future surface mass balance (SMB) of the Greenland ice sheet (GrIS) is to force a regional climate model (RCM), typically running at 5 to 10 km horizontal resolution, at the lateral and top boundaries with the output of an Earth System Model (ESM; ∼100 km) (Van Angelen et al., 2013a; Fettweis et al., 2013; Mottram et al., 2017). However, ESMs from the fifth phase of the Climate Model Intercomparison Project (CMIP5) do not accurately represent the contemporary large-scale climate of the Greenland region (Rae et al., 2012; Fettweis et al., 2013). The reason is that ESMs do not assimilate nor prescribe climatic observations as do global climate reanalyses (Uppala et al., 2005; Dee et al., 2011) and RCMs (Fettweis et al., 2017; Mottram et al., 2017; Niwano et al., 2018; Noël et al., 2018). For instance, ESMs fail at capturing the recent summertime Arctic atmospheric circulation change (Hanna et al., 2018), making projections of GrIS mass loss and

contribution to sea level rise highly uncertain (Delhasse et al., 2018). Consequently, climate forcing from CMIP5 ESMs still requires dedicated bias correction before being used to force RCMs over the GrIS (Rae et al., 2012; Fettweis et al., 2013; Van Angelen et al., 2013a). An alternative approach is to directly use outputs of ESMs to estimate GrIS SMB; however, most ESMs do not have (sophisticated) snow models that consider meltwater retention in firn, while their coarse spatial resolution does not

5   accurately resolve the large SMB gradients at the GrIS margins (Lenaerts et al., 2019).

Here, we use the historical climate (1950-2014) of a CMIP6 model, the Community Earth System Model version 2.1 (CESM2; ∼111 km), to force the lateral and top boundaries of the Regional Atmospheric Climate Model version 2.3p2 (RACMO2; ∼11 km). The reason for selecting CESM2 as the climate forcing for RACMO2 stems from the active involvement of the Institute for Marine and Atmospheric research Utrecht (IMAU) in the development and improvement of the model for

10   studies over both the Greenland and Antarctic ice sheets. To obtain a meaningful comparison with in situ observations, the resulting SMB field is then statistically downscaled to 1 km over the GrIS and peripheral glaciers and ice caps (Fig. 1a) (Noël et al., 2018). We show that, without additional corrections, CESM2 climate forcing yields a realistic reconstruction of historical GrIS SMB (1950-2014), including the recent acceleration in mass loss. This is unexpected for an ESM which is exclusively driven by prescribing greenhouse gas (CO_2 and CH_4) and aerosol emissions, and may herald more accurate projections of GrIS

15   contribution to future sea level rise. Section 2 describes CESM2 and RACMO2, including model initialisation, forcing set-up, as well as observational and model data sets used for evaluation. Section 3 evaluates the CESM2-forced RACMO2 product using in situ and remotely sensed measurements. Model comparison to previous RACMO2 simulations is discussed in Section 4, as well as representation of recent trends in SMB components and mass loss. Conclusions are drawn in Section 5.

2   Methods

20   **2.1   Community Earth System Model: CESM2**

CESM2.1, hereafter referred to as CESM2, is an ESM that simulates mutual interactions between atmosphere-ocean-land systems on the global scale. The model incorporates the Community Atmosphere Model version 6 (CAM6) (Gettelman et al., 2019), resolving global atmospheric dynamics and physics; the Parallel Ocean Program model version 2.1 (POP2.1) (Smith et al., 2010) and the Los Alamos National Laboratory Sea Ice Model version 5.1 (CICE5.1) (Bailey et al., 2018),

25   modelling global oceanic circulation and sea-ice evolution. These are coupled with the Community Land Model version 5 (CLM5) (Lawrence, 2019) and the Community Ice Sheet Model version 2.1 (CISM2.1) (Lipscomb et al., 2019) simulating land-atmosphere interactions and ice dynamics. Here, we use a full atmosphere-ocean coupling in CESM2, i.e. including sea ice dynamics and sea surface temperature evolution while excluding land ice dynamics (e.g. calving). The model is run at 1° spatial resolution (∼111 km) and only prescribes atmospheric greenhouse gas (CO_2 and CH_4) and aerosol emissions as well

30   as land cover use (Eyring et al., 2016). CESM2 has been extensively tested and adapted to realistically reproduce the contemporary climate and SMB of the GrIS (Van Kampenhout et al., 2017, 2019b), detailed model description and latest updates are provided in Van Kampenhout et al. (2019a).

2.2 Regional Atmospheric Climate Model: RACMO2

RACMO2 is an RCM that is specifically adapted to simulate the climate of polar ice sheets (Noël et al., 2018; Van Wessem et al., 2018). The model incorporates the dynamical core of the High Resolution Limited Area Model (HIRLAM) (Undèn et al., 2002) and the physics package cycle CY33r1 of the European Centre for Medium-range Weather Forecasts Integrated Forecast System (ECMWF-IFS, 2008). It includes a multi-layer snow module that simulates melt, liquid water percolation and retention, refreezing and runoff (Ettema et al., 2010), and accounts for dry snow densification following Ligtenberg et al. (2011). RACMO2 implements an albedo scheme that calculates snow albedo based on prognostic snow grain size, cloud optical thickness, solar zenith angle and impurity concentration in snow (Kuipers Munneke et al., 2011). In line with in situ measurements (Doherty et al., 2010), impurity concentration (soot) in RACMO2 is prescribed as a constant in time and space at 0.1 ppmv (Noël et al., 2018). The model simulates drifting snow erosion and sublimation following Lenaerts et al. (2012). The latest model version RACMO2.3p2 accurately simulates the contemporary climate and SMB of the GrIS when forced by ERA-40 (1958-1978) and ERA-Interim (1979-present) climate reanalyses (Uppala et al., 2005; Dee et al., 2011) and statistically downscaled to 1 km (see Section 2.4). For detailed model description and latest updates, we refer to Noël et al. (2018, 2019).

2.3 Model initialisation and set-up

Here, we conduct a CMIP6-style historical simulation (1950-2014) using RACMO2.3p2 at 11 km horizontal resolution (Noël et al., 2018) to dynamically downscale the output of CESM2 prescribed in a 24 grid-cell wide relaxation zone at the model lateral boundaries. Forcing consists of atmospheric temperature, pressure, specific humidity, wind speed and direction being prescribed on a 6-hourly basis at the 40 model atmospheric levels. Upper atmosphere relaxation is implemented (Van de Berg and Medley, 2016). Sea surface temperature and sea ice extent/cover are also prescribed from the CESM2 forcing every 6 hours. RACMO2.3p2 has typically 40 to 60 active snow layers that are initialised in January 1950 using temperature and density profiles derived from the offline IMAU Firn Densification Model (IMAU-FDM) (Ligtenberg et al., 2018). Glacier outlines and surface topography are prescribed from a down-sampled version of the 90 m Greenland Ice Mapping Project (GIMP) Digital Elevation Model (DEM) (Howat et al., 2014). Bare ice albedo is prescribed from the 500 m MODerate-resolution Imaging Spectroradiometer (MODIS) 16-day Albedo product (MCD43A3), as the 5% lowest surface albedo records for the period 2000-2015, clipped between 0.30 for bare ice and 0.55 for bright ice covered by perennial firn in the accumulation zone. The current study uses the climate forcing of one out of the twelve members of the CESM2 historical ensemble. Forcing RACMO2 with other CESM2 members would have been ideal, but doing so in a transient fashion and at high spatial and temporal resolution is computationally prohibitive. Instead, we select one member that offers the 6-hourly climate forcing required to drive RACMO2 while being representative of other CESM2 members (see Section 4.3 and Fig. 4a).

2.4 Statistical downscaling

Following Noël et al. (2016), the historical simulation at 11 km, hereafter referred to as CESM2-forced RACMO2.3p2, is further statistically downscaled to a 1 km ice mask and topography derived from the 90 m GIMP DEM (Howat et al., 2014).

In brief, the downscaling procedure corrects individual SMB components (except for precipitation), i.e. primarily meltwater runoff, for elevation and ice albedo biases on the relatively coarse model grid at 11 km resolution. These corrections reconstruct individual SMB components on the 1 km GrIS topography using daily-specific gradients estimated at 11 km, and minimise the remaining runoff underestimation using a down-sampled 1 km MODIS 16-day ice albedo product averaged for 2000-2015.

5 Precipitation, including snowfall and rainfall, is bi-linearly interpolated from the 11 km onto the 1 km grid without additional corrections (Noël et al., 2018). Statistical downscaling proves essential to resolve narrow ablation zones, outlet glaciers and ice caps at the GrIS margins that significantly contribute to contemporary mass loss of Greenland land ice (Noël et al., 2017, 2019). For instance, applying statistical downscaling increases GrIS-wide runoff by 55 Gt yr^{-1} (+23%) on average for the period 1950-2014, resulting in a SMB decrease of 56 Gt yr^{-1} (-13%).

2.5 Evaluation data sets

For evaluation, we use a compilation of in situ SMB measurements derived from 182 stakes, snow pits (Bales et al., 2009) and airborne radar campaign (Overly et al., 2016) in the GrIS accumulation area (182 records; white dots in Fig. 1a), and collected at 213 sites (Machguth et al., 2016) in the ablation zone (1073 records; yellow dots in Fig. 1a). In addition, combined modelled SMB and glacial discharge estimates (Mouginot et al., 2019) are compared to mass changes from GRACE over the

15 period 2003-2014 (Wouters et al., 2013). The CESM2-forced RACMO2.3p2 historical simulation is also compared to SMB and individual components from an ensemble of eight previous RACMO2 simulations (Van Angelen et al., 2013a, b; Noël et al., 2015, 2016, 2018, 2019), using different climate forcing (ERA-reanalysis or the ESM HadGEM2) at various spatial resolutions (1, 5.5 and 11 km). These simulations are listed and further compared in Tables A1 and A2 for the overlapping model period 1960-2012.

3 Surface mass balance evaluation and uncertainty

Figure 1a shows annual mean SMB from CESM2-forced RACMO2.3p2, statistically downscaled to 1 km. As is the case with state-of-the-art reanalysis-forced simulations (Mottram et al., 2017; Fettweis et al., 2017; Niwano et al., 2018; Noël et al., 2018, 2019), it accurately captures the extensive inland accumulation area, and narrow ablation zones, outlet glaciers and ice caps fringing the GrIS margins (Fig. 1a). The model shows very good agreement with multi-year averaged SMB observations in the accumulation zone (R^2 = 0.89; Fig. 1b), with a small bias and RMSE of -20.5 mm w.e. and 63.3 mm w.e. Interestingly, these statistics are on par with the most recent RACMO2.3p2 run forced by ERA-reanalysis and statistically downscaled to 1 km (Noël et al., 2018), hereafter referred to as ERA-forced RACMO2.3p2.

In the ablation zone, CESM2-forced RACMO2.3p2 agrees reasonably well with ablation measurements: R^2 = 0.61 vs. 0.72 (Noël et al., 2018) (Fig. 1c). The model shows larger bias and RMSE relative to ERA-forced RACMO2.3p2 (+0.06 m w.e. and +0.18 m w.e.). As CESM2 does not assimilate nor prescribe climatic observations, a larger bias was expected. Good agreement with observations can be partly attributed to dynamical downscaling in RACMO2, that results in realistic SMB gradients if appropriate climate forcing is prescribed (Noël et al., 2018); and to statistical downscaling, as it minimises SMB

bias by enhancing runoff in marginal ablation zones (Noël et al., 2016). On the regional scale, CESM2-forced and ERA-forced RACMO2.3p2 simulations show no significant difference in SMB and components for the period 1958-2014 (not shown), i.e. mean difference (CESM2-forced minus ERA-forced) lower than one standard deviation of the 1958-2014 period.

We follow Noël et al. (2017) to estimate the SMB uncertainty (σ). Mean accumulation (20.5 mm w.e.; Fig. 1b) and ablation
5   biases (180.0 mm w.e.; Fig. 1c) are accumulated over the long-term (1958-2014) accumulation and ablation zone of the GrIS, with an area of $\sim$1,521,400 km^2 and $\sim$179,400 km^2 respectively:

$$\sigma = \sqrt{(bias^{\text{ abl.}} \times area^{\text{ abl.}})^2 + (bias^{\text{ acc.}} \times area^{\text{ acc.}})^2} \tag{1}$$

This yields σ = 48 Gt yr^{-1}. A similar value (43 Gt yr^{-1}) is obtained for the downscaled ERA-forced RACMO2.3p2 product. Integrated over the ice sheet, CESM2-forced and ERA-forced simulations agree very well, with an average cumulative SMB
10   of 365 $\pm$ 48 Gt yr^{-1} and 357 $\pm$ 43 Gt yr^{-1} for the period 1958-2014. Figure 1d compares modelled and remotely sensed (GRACE) cumulative mass change for the period 2003-2014, respectively. Modelled mass change (-3,299 $\pm$ 1,240 Gt; blue box), estimated as cumulative SMB over the GrIS, peripheral ice caps and tundra region (2,970 $\pm$ 1,097 Gt; black box) minus glacial discharge (6,269 $\pm$ 143 Gt; orange box), shows excellent agreement with GRACE (-3,290 $\pm$ 1,434 Gt; red box). This highlights the ability of CESM2-forced RACMO2.3p2 to also realistically capture the recent Greenland mass loss (2003-2014)
15   (Bamber et al., 2018).

4   Surface mass balance variability

Figures 2a and c show annual mean SMB components simulated by CESM2-forced RACMO2.3p2 at 1 km (horizontal bars) for the periods 1960-1990 and 1991-2012. Likewise, Figs. 2b and d show annual mean mass balance (MB; blue), i.e. SMB (black) minus glacial discharge (orange), simulated by CESM2-forced RACMO2.3p2 on the original model grid (11 km) and
20   statistically downscaled to 1 km for the two periods. Ice discharge and associated uncertainties (1972-2014) are from Mouginot et al. (2019). Prior to 1972, ice discharge and uncertainties are assumed constant at the 1972 value. Error bars represent the inter-annual variability in SMB components estimated as one standard deviation around the mean. Boxes show the range of modelled SMB components derived from the ensemble of RACMO2 simulations forced by ERA-reanalysis. Annual mean SMB components and corresponding inter-annual variability for the ensemble RACMO2 simulations are listed in Tables A1
25   (1960-1990) and A2 (1991-2012).

4.1   Approximate mass balance: 1960-1990

In the period 1960-1990, the mass balance of the GrIS was close to zero (Van den Broeke et al., 2016) or slightly negative (Mouginot et al., 2019). Figures 2a, b and Table A1 show that downscaled CESM2-forced RACMO2.3p2 reproduces, within one standard deviation, SMB and components obtained from eight previous reanalysis-forced RACMO2 simulations at various
30   spatial resolutions. For instance, precipitation (701 $\pm$ 98 Gt yr^{-1}) and runoff (242 $\pm$ 40 Gt yr^{-1}) compare well with ERA-

forced RACMO2.3p2 (Noël et al., 2018), i.e. 712 ± 73 Gt yr^{-1} and 257 ± 53 Gt yr^{-1}, resulting in similar SMB of 428 and 423 Gt yr^{-1} (-1%) (Fig. 2a and Table A1). This highlights the ability of the CESM2 forcing to capture realistic Greenland SMB before mass loss started in the 1990s.

Figure 2b shows that SMB on the 11 km grid falls well within ERA-forced simulations at similar resolution (black box). Through statistical downscaling, SMB at 1 km decreases by 13% from 485 to 428 Gt yr^{-1}, in line with other simulations (Fig. 2b and Table A1). Combining average GrIS-integrated SMB with glacial discharge (458 Gt yr^{-1}; 1960-1990), CESM2-forced RACMO2.3p2 results in slightly negative mass balance (-31 Gt yr^{-1}; Table A1). A previous attempt using RACMO2.1 forced by the climate of the HadGEM2 ESM (Van Angelen et al., 2013a) did not accurately represent GrIS-integrated SMB components (dark green dots in Figs. 2a,b). While precipitation was generally well represented (685 ± 82 Gt yr^{-1}), runoff was overestimated by $\sim$50% compared to ERA-forced RACMO2.3p2 (Table A1). As a result, SMB was underestimated by $\sim$40%, driving an unrealistic mass loss of 189 Gt yr^{-1} over the period 1960-1990. For additional information about the HadGEM2-forced RACMO2.1 simulation and settings, we refer the reader to Van Angelen et al. (2013a); key differences between RACMO2.1, RACMO2.3p1 and p2 are discussed in Noël et al. (2015, 2018).

4.2 Mass loss: 1991-2012

In the two decades following 1990 (1991-2012), the GrIS experienced accelerated mass loss (Bamber et al., 2018; Shepherd et al., 2019), primarily driven by a decrease in SMB (-138 Gt yr^{-1} with respect to 1960-1990; Fig. 2c and Table A2) combined with an increase in glacial discharge (+26 Gt yr^{-1}). Figure 2c shows that CESM2-forced RACMO2.3p2 similarly reproduces the recent SMB decrease resulting from enhanced surface runoff (+138 Gt yr^{-1} or +57%) compared to the ERA-forced RACMO2.3p2 simulation (+100 Gt yr^{-1} or +38%). This pronounced runoff increase stems from enhanced surface melt (+163 Gt yr^{-1} or +36%) exceeding the increase in meltwater retention and refreezing in the firn (+36 Gt yr^{-1} or +14%). Precipitation does not substantially change after 1991, in line with the ensemble ERA-forced RACMO2 simulations (Table A2). We conclude that CESM2-forced RACMO2.3p2 captures the post-1990 SMB decrease that tipped the GrIS into a state of sustained mass loss (195 Gt yr^{-1} and 170 Gt yr^{-1} for downscaled CESM2-forced and ERA-forced RACMO2.3p2 for 1991-2012; Fig. 2d). In contrast, SMB components in HadGEM2-forced RACMO2.1 remain largely overestimated compared to other simulations (Table A2), particularly runoff and melt (Fig. 2c), resulting in overestimated mass loss for 1991-2012 (240 ± 80 Gt yr^{-1}; Fig. 2d). The reason is that, unlike CESM2 (Van Kampenhout et al., 2019a), the HadGEM2 forcing had a strong, systematic warm bias of $\sim$1°C (Van Angelen et al., 2013a), resulting in overestimated meltwater runoff and thus underestimated SMB (Fig. 2d).

4.3 Time series and trends

Figures 3a and b show time series of individual GrIS-integrated SMB components for the period 1950-2014 as modelled by the latest, state-of-the-art ERA-forced RACMO2.3p2 run at 5.5 km horizontal resolution (Noël et al., 2019) and the current CESM2-forced RACMO2.3p2 simulation, both statistically downscaled to 1 km. It is important to note that, compared to forcing by reanalyses that assimilate observations, the CESM2-forced simulation produces extreme melt years (e.g. 2005 and

6

2011; Fig. 3b) that are realistic in magnitude but not necessarily in timing (e.g. the observed 2012 melt peak; Fig. 3a). For 1960-1990, the two products show similar and insignificant trends in total precipitation (2.4 ± 1.6 Gt yr^{-2}; p-value = 0.14) and runoff (1.1 ± 1.0 Gt yr^{-2}; p-value = 0.27) (Fig. 3b). After 1991, CESM2-forced RACMO2.3p2 reproduces the significant (p-value = 0.0001) positive runoff trend (10.4 ± 2.2 Gt yr^{-2}; Fig. 3b) similar to the ERA-forced simulation (8.8 ± 2.1 Gt yr^{-2};

5   Fig. 3a). The runoff trend in CESM2-forced RACMO2.3p2 is no coincidence. Figure 4a shows the atmospheric temperature at 700 hPa (T_{700}) from the current CESM2 simulation (red) and from 11 additional ensemble members (grey). Compared to T_{700} derived from ERA-40 (1958-1978) and ERA-Interim (1979-2014; black line in Fig. 4a), the current CESM2 simulation shows a cold bias of 0.6^oC over 1958-2014. For the ERA-Interim period, the bias decreases to 0.4^oC. All CESM2 members show a similar warming trend after 1991, in line with the reanalysis data (dashed black line), highlighting the ability of CESM2 to

10   represent the recent climate of Greenland. As in Fettweis et al. (2013), we find a clear correlation (r = 0.67; Fig. 4b) between CESM2-forced RACMO2.3p2 runoff at 1 km and T_{700} from the CESM2 simulation (red). This means that the post-1990 runoff increase would have been obtained irrespective of the selected CESM2 member. Physical drivers of the warming trend in the CESM2 forcing are currently being investigated and will be discussed in a forthcoming publication. Compared to the ERA-forced run, the more pronounced runoff trend in CESM2-forced RACMO2.3p2 results from a significant (p-value = 0.016)

15   positive trend in rainfall (1.3 ± 0.3 Gt yr^{-2} vs. 0.3 ± 0.2 Gt yr^{-2}) for a similar melt acceleration (11.9 ± 3.0 Gt yr^{-2} vs. 10.9 ± 3.0 Gt yr^{-2}). Total precipitation in the CESM2-forced RACMO2.3p2 simulation shows a significant (p-value = 0.002) positive trend (5.8 ± 1.7 Gt yr^{-2}; Fig. 3b) in contrast to a negative trend in the ERA-forced run (-1.9 ± 1.8 Gt yr^{-2}; Fig. 3a). However, the latter trend stems from decadal variability as it becomes insignificant for the period 1950-2014: 0.9 ± 0.5 Gt yr^{-2} (p-value = 0.090). In addition, the positive precipitation trend disappears when extending time series using a CESM2-based

20   SSP8.5 scenario (not shown), demonstrating that the latter trend originates from internal decadal variability.

    In line with Van den Broeke et al. (2016), Fig. 3c shows that $\sim60\%$ of the recent mass loss acceleration in CESM2-forced RACMO2.3p2 is caused by decreased SMB (6.6 ± 3.3 Gt yr^{-2}) resulting from enhanced meltwater runoff; the remaining $\sim40\%$ is ascribed to increased glacial discharge (4.7 ± 0.5 Gt yr^{-2}). As a result, Greenland mass balance decreased by an estimated rate of 11.3 ± 3.2 Gt yr^{-2} (or 9.4 ± 1.6 Gt yr^{-2} for the GrIS only) in good agreement with GRACE (9.4 ± 1.2

25   Gt yr^{-2} for 2003-2014; Fig. 3c). This is meaningful for two reasons: for the first time, an ESM, assimilating no observational climatic data except for atmospheric greenhouse gas and aerosol emissions, can 1) reliably reproduce the historical average and variability of SMB and its individual components; 2) accurately represent the recent Greenland mass loss acceleration. These results are essential for forthcoming attribution studies investigating post-1990 GrIS mass loss.

5   Conclusions

30   Historical output (1950-2014) of the Earth System Model CESM2 (~111 km) is dynamically downscaled using the regional climate model RACMO2.3p2 (~11 km) over the GrIS. The resulting SMB components are further statistically downscaled to 1 km spatial resolution to resolve the narrow ablation zones and marginal outlet glaciers of Greenland. Model evaluation using in-situ and remotely sensed measurements demonstrates the ability of CESM2-forced RACMO2.3p2 to accurately

reproduce SMB as well as the rapid post-1991 melt and runoff increase. Combining modelled SMB with observed glacial discharge, our new ESM-based SMB product reflects an ice sheet in approximate mass balance before 1991, followed by a rapid mass loss acceleration resulting from enhanced meltwater runoff: two key features that, until now, exclusively showed up in reanalysis-based estimates. This means that, for the first time, an Earth System Model (CESM2), that does not assimilate

5   climatic observations, can be used to force a regional climate model (RACMO2) to accurately reproduce historical GrIS SMB average and variability. Furthermore, our results suggest that CESM2 climate forcing can be used without bias corrections to simulate the climate and SMB of the GrIS for different warming scenario projections to quantify the GrIS contribution to future eustatic sea level rise.

References

Bailey, D., Hunke, E., DuVivier, A., Lipscomb, B., Bitz, C., Holland, M., Briegleb, B., and Schramm, J.: CESM CICE5 Users Guide, Release CESM CICE5, Documentation and Software User's Manual from Los Alamos National Laboratory, pp. 1 – 41, http://www.cesm.ucar.edu/models/cesm2/sea-ice/, 2018.

Bales, R. C., Guo, Q., Shen, D., McConnell, J. R., Du, G., Burkhart, J. F., Spikes, V. B., Hanna, E., and Cappelen, J.: Annual accumulation for Greenland updated using ice core data developed during 2000-2006 and analysis of daily coastal meteorological data, Journal of Geophysical Research, 114, D06 116, https://doi.org/10.1029/2008JD011208, 2009.

Bamber, J. L., Westaway, R. M., Marzeion, B., and Wouters, B.: The land ice contribution to sea level during the satellite era, Environmental Research Letters, 13, 063 008, https://doi.org/10.1088/1748-9326/aac2f0, 2018.

Dee, D. P., Uppala, S. M., Simmons, A. J., Berrisford, P., Poli, P., Kobayashi, S., Andrae, U., Balmaseda, M. A., Balsamo, G., Bauer, P., Bechtold, P., Beljaars, A. C. M., van de Berg, L., Bidlot, J., Bormann, N., Delsol, C., Dragani, R., Fuentes, M., Geer, A. J., Haimberger, L., Healy, S. B., Hersbach, H., Hòlm, E. V., Isaksen, L., Kållberg, P., Köhler, M., Matricardi, M., McNally, A. P., Monge-Sanz, B. M., Morcrette, J.-J., Park, B.-K., Peubey, C., de Rosnay, P., Tavolato, C., Thépaut, J.-N., and Vitart, F.: The ERA-Interim reanalysis: configuration and performance of the data assimilation system, Quarterly Journal of the Royal Meteorological Society, 137, 553 – 597, https://doi.org/10.1002/qj.828, 2011.

Delhasse, A., Fettweis, X., Kittel, C., Amory, C., and Agosta, C.: Brief communication: Impact of the recent atmospheric circulation change in summer on the future surface mass balance of the Greenland ice sheet, The Cryosphere, 12, 3409–3418, https://doi.org/10.5194/tc-12-3409-2018, 2018.

Doherty, S. J., Warren, S. G., Grenfell, T. C., Clarke, A. D., , and Brandt, R. E.: Light-absorbing impurities in Arctic snow, Atmos. Chem. Phys., 10, 11 647 – 11 680, https://doi.org/10.5194/acp-10-11647-2010, 2010.

ECMWF-IFS: Part IV : PHYSICAL PROCESSES (CY33R1), Technical Report, 2008.

Ettema, J., van den Broeke, M. R., van Meijgaard, E., van de Berg, W. J., Box, J. E., and Steffen, K.: Climate of the Greenland ice sheet using a high-resolution climate model - Part 1: Evaluation, The Cryosphere, 4, 511 – 527, https://doi.org/10.5194/tc-4-511-2010, 2010.

Eyring, V., Bony, S., Meehl, G. A., Senior, C. A., Stevens, B., Stouffer, R. J., and Taylor, K. E.: Overview of the Coupled Model Intercomparison Project Phase 6 (CMIP6) experimental design and organization, Geosci. Model Dev., 9, 1937 – 1958, https://doi.org/10.5194/gmd-9-1937-2016, 2016.

Fettweis, X., Franco, B., Tedesco, M., van Angelen, J. H., Lenaerts, J. T. M., van den Broeke, M. R., and Gallée, H.: Estimating the Greenland ice sheet surface mass balance contribution to future sea level rise using the regional atmospheric climate model MAR, The Cryosphere, 7, 469 – 489, https://doi.org/10.5194/tc-7-469-2013, 2013.

Fettweis, X., Box, J. E., Agosta, C., Amory, C., Kittel, C., Lang, C., van As, D., Machguth, H., and Gallée, H.: Reconstructions of the 1900-2015 Greenland ice sheet surface mass balance using the regional climate MAR model, The Cryosphere, 11, 1015 – 1033, https://doi.org/10.5194/tc-11-1015-2017, 2017.

Gettelman, A., Truesdale, J. E., Bacmeister, J. T., Caldwell, P. M., Neale, R. B., Bogenschutz, P. A., and Simpson, I. R.: The Single Column Atmosphere Model Version 6 (SCAM6): Not a Scam but a Tool for Model Evaluation and Development, Journal of Advances in Modeling Earth Systems, 11, 1381 – 1401, https://doi.org/10.1029/2018MS001578, 2019.

Hanna, E., Fettweis, X., and Hall, R. J.: Brief communication: Recent changes in summer Greenland blocking captured by none of the CMIP5 models, The Cryosphere, 12, 3287 – 3292, https://doi.org/10.5194/tc-12-3287-2018, 2018.

Howat, I. M., Negrete, A., and Smith, B. E.: The Greenland Ice Mapping Project (GIMP) land classification and surface elevation data sets, The Cryosphere, 8, 1509 – 1518, https://doi.org/10.5194/tc-8-1509-2014, 2014.

Kuipers Munneke, P., van den Broeke, M. R., Lenaerts, J. T. M., Flanner, M. G., Gardner, A. S., and van de Berg, W. J.: A new albedo parameterization for use in climate models over the Antarctic ice sheet, Journal of Geophysical Research, 116, D05 114, https://doi.org/10.1029/2010JD015113, 2011.

5   Lawrence, D.: The Community Land Model version 5: Description of new features, benchmarking, and impact of forcing uncertainty, Journal of Advances in Modeling Earth Systems, in press, 2019.

Lenaerts, J. T. M., van den Broeke, M. R., Angelen, J. H., van Meijgaard, E., and Déry, S. J.: Drifting snow climate of the Greenland ice sheet: a study with a regional climate model, The Cryosphere, 6, 891 – 899, https://doi.org/10.5194/tc-6-891-2012, 2012.

Lenaerts, J. T. M., Medley, B., van den Broeke, M. R., and Wouters, B.: Observing and Modeling Ice Sheet Surface Mass Balance, Reviews

10   of Geophysics, 57, 376 – 420, https://doi.org/10.1029/2018RG000622, 2019.

Ligtenberg, S. R. M., Helsen, M. M., and van den Broeke, M. R.: An improved semi-empirical model for the densification of Antarctic firn, The Cryosphere, 5, 809 – 819, https://doi.org/10.5194/tc-5-809-2011, 2011.

Ligtenberg, S. R. M., Munneke, P. K., Noël, B., and van den Broeke, M. R.: Brief communication: Improved simulation of the present-day Greenland firn layer (1960-2016), The Cryosphere, 12, 1643 – 1649, https://doi.org/10.5194/tc-12-1643-2018, 2018.

15   Lipscomb, W. H., Price, S. F., Hoffman, M. J., Leguy, G. R., Bennett, A. R., Bradley, S. L., Evans, K. J., Fyke, J. G., Kennedy, J. H., Perego, M., Ranken, D. M., Sacks, W. J., Salinger, A. G., Vargo, L. J., and Worley, P. H.: Description and evaluation of the Community Ice Sheet Model (CISM) v2.1, Geoscientific Model Development, 12, 387 – 424, https://doi.org/10.5194/gmd-12-387-2019, 2019.

Machguth, H., Thomsen, H., Weidick, A., Ahlstrøm, A. P., Abermann, J., Andersen, M. L., Andersen, S., Bjørk, A. A., Box, J. E., Braithwaite, R. J., Bøggild, C. E., Citterio, M., Clement, P., Colgan, W., Fausto, R. S., Gubler, K. G. S., Hasholt, B., Hynek, B., Knudsen, N., Larsen,

20   S., Mernild, S., Oerlemans, J., Oerter, H., Olesen, O., Smeets, C., Steffen, K., Stober, M., Sugiyama, S., van As, D., van den Broeke, M., and van de Wal, R. S.: Greenland surface mass balance observations from the ice sheet ablation area and local glaciers, Journal of Glaciology, pp. 1 – 27, https://doi.org/10.1017/jog.2016.75, 2016.

Mottram, R., Boberg, F., Langen, P., Yang, S., Rodehacke, C., Christensen, J. H., and Madsen, M. S.: Surface Mass balance of the Greenland ice Sheet in the Regional Climate Model HIRHAM5: Present State and Future Prospects, Low Temperature Science, 75, 105 – 115,

25   https://doi.org/10.14943/lowtemsci.75.105, 2017.

Mouginot, J., Rignot, E., Bjørk, A., van den Broeke B., M., Millan, R., Morlighem, M., Noël, B., Scheuchla, and Wood, M.: Forty six years of Greenland Ice Sheet mass balance from the component method: 1972 to 2018, PNAS, in press., 2019.

Niwano, M., Aoki, T., Hashimoto, A., Matoba, S., Yamaguchi, S., Tanikawa, T., Fujita, K., Tsushima, A., Iizuka, Y., Shimada, R., and Hori, M.: NHM-SMAP: spatially and temporally high-resolution nonhydrostatic atmospheric model coupled with detailed snow process model

30   for Greenland Ice Sheet, The Cryosphere, 12, 635 – 655, https://doi.org/10.5194/tc-12-635-2018, 2018.

Noël, B., van de Berg, W. J., van Meijgaard, E., Munneke, P. K., van de Wal, R. S. W., and van den Broeke, M.: Evaluation of the updated regional climate model RACMO2.3: summer snowfall impact on the Greenland Ice Sheet, The Cryosphere, 9, 1831 – 1844, https://doi.org/10.5194/tc-9-1831-2015, 2015.

Noël, B., van de Berg, W. J., Machguth, H., Lhermitte, S., Howat, I., Fettweis, X., and van den Broeke, M. R.: A daily, 1 km resolution data

35   set of downscaled Greenland ice sheet surface mass balance (1958-2015), The Cryosphere, 10, 2361 – 2377, https://doi.org/10.5194/tc-10-2361-2016, 2016.

Noël, B., van de Berg, W. J., Lhermitte, S., Wouters, B., Machguth, H., Howat, I., Citterio, M., Moholdt, G., Lenarets, J. T. M., and van den Broeke, M. R.: A tipping point in refreezing accelerates mass loss of Greenland's glaciers and ice caps, Nature Communications, 8, 14 730, https://doi.org/10.1038/ncomms14730, 2017.

Noël, B., van de Berg, W. J., van Wessem, J. M., van Meijgaard, E., van As, D., Lenaerts, J. T. M., Lhermitte, S., Munneke, P. K., Smeets, C. J. P. P., van Ulft, L. H., van de Wal, R. S. W., and van den Broeke, M. R.: Modelling the climate and surface mass balance of polar ice sheets using RACMO2, Part 1: Greenland (1958-2016), The Cryosphere, 12, 811 – 831, https://doi.org/10.5194/tc-12-811-2018, 2018.

Noël, B., van de Berg, W. J., Lhermitte, S., and van den Broeke, M. R.: Rapid ablation zone expansion amplifies north Greenland mass loss, Science Advances, 5, eaaw0123, https://doi.org/10.1126/sciadv.aaw0123, 2019.

Overly, T. B., Hawley, R. L., Helm, V., Morris, E. M., and Chaudhary, R. N.: Greenland annual accumulation along the EGIG line, 1959-2004, from ASIRAS airborne radar and detailed neutron-probedensity measurements, The Cryosphere, 10, 1679 – 1694, https://doi.org/10.5194/tc-10-1679-2016, 2016.

Rae, J. G. L., Aõalgeirsdóttir, G., Edwards, T. L., Fettweis, X., Gregory, J. M., Hewitt, H. T., Lowe, J. A., Lucas-Picher, P., Mottram, R. H., Payne, A. J., Ridley, J. K., Shannon, S. R., van de Berg, W. J., van de Wal, R. S. W., and van den Broeke, M. R.: Greenland ice sheet surface mass balance: evaluating simulations and making projections with regional climate models, The Cryosphere, 6, 1275 – 1294, https://doi.org/10.5194/tc-6-1275-2012, 2012.

Shepherd, A., Ivins, E., and et al., E. R.: Mass balance of the Greenland Ice Sheet from 1992 to 2018, Nature, p. 25 pp., https://doi.org/10.1038/s41586-019-1855-2, 2019.

Smith, R., Jones, P., Briegleb, B., Bryan, F., Danabasoglu, G., Dennis, J., Dukowicz, J., Eden, C., Fox-Kemper, B., and Gent, P.: The parallel ocean program (POP) reference manual ocean component of the community climate system model (CCSM) and community earth system model (CESM), Rep. LAUR-01853, 141, 1 – 140, 2010.

Undèn, P., Rontu, L., Järvinen, H., Lynch, P., Calvo, J., Cats, G., Cuxart, J., Eerola, K., Fortelius, C., Garcia-Moya, J. A., Jones, C., Lenderlink, G., Mcdonald, A., Mcgrath, R., Navascues, B., Nielsen, N. W., Degaard, V., Rodriguez, E., Rummukainen, M., Sattler, K., Sass, B. H., Savijarvi, H., Schreur, B. W., Sigg, R., and The, H.: HIRLAM-5, Scientific Documentation, technical Report, 2002.

Uppala, S. M., Kållberg, P. W., Simmons, A. J., Andrae, U., Bechtold, V. D. C., Fiorino, M., Gibson, J. K., Haseler, J., Hernandez, A., Kelly, G. A., Li, X., Onogi, K., Saarinen, S., Sokka, N., Allan, R. P., Andersson, E., Arpe, K., Balmaseda, M. A., Beljaars, A. C. M., Berg, L. V. D., Bidlot, J., Bormann, N., Caires, S., Chevallier, F., Dethof, A., Dragosavac, M., Fisher, M., Fuentes, M., Hagemann, S., Hòlm, E., Hoskins, B. J., Isaksen, L., Janssen, P. A. E. M., Jenne, R., Mcnally, A. P., Mahfouf, J.-F., Morcrette, J.-J., Rayner, N. A., Saunders, R. W., Simon, P., Ster, A., Trenberth, K. E., Untch, A., Vasiljevic, D., Viterbo, P., and Woollen, J.: The ERA-40 re-analysis, Quarterly Journal of the Royal Meteorological Society, 131, 2961 – 3012, 2005.

Van Angelen, J. H., Lenaerts, J. T. M., van den Broeke, M. R., Fettweis, X., and van Meijgaard, E.: Rapid loss of firn pore space accelerates 21st century Greenland mass loss, Geophysical Research Letters, 40, 2109 – 2113, https://doi.org/10.1002/grl.50490, 2013a.

Van Angelen, J. H., van den Broeke, M. R., Wouters, B., and Lenaerts, J. T. M.: Contemporary (1969-2012) evolution of the climate and surface mass balance of the Greenland ice sheet, Surveys in Geophysics, 35, 1155 – 1174, https://doi.org/10.1007/s10712-013-9261-z, 2013b.

Van de Berg, W. J. and Medley, B.: Brief Communication: Upper-air relaxation in RACMO2 significantly improves modelled interannual surface mass balance variability in Antarctica , The Cryosphere, 10, 459 – 463, https://doi.org/https://doi.org/10.5194/tc-10-459-2016, 2016.

Van den Broeke, M. R., Enderlin, E., Howat, I., Munneke, P. K., Noël, B., van de Berg, W. J., van Meijgaard, E., and Wouters, B.: On the recent contribution of the Greenland ice sheet to sea level change, The Cryosphere, 10, 1933 – 1946, https://doi.org/10.5194/tc-10-1933-2016, 2016.

Van Kampenhout, L., Rhoades, A. M., Herrington, A. R., Zarzycki, C. M., Lenaerts, J. T. M., Sacks, W. J., and van den Broeke, M. R.: Improving the Representation of Polar Snow and Firn in the Community Earth System Model, Journal of Advances in Modeling Earth
5   Systems, 9, 2583 – 2600, https://doi.org/10.1002/2017MS000988, 2017.

Van Kampenhout, L., Lenaerts, J. T. M., Lipscomb, W. H., Lhermitte, S., Noël, B., Vizcaíno, M., Sacks, W. J., and van den Broeke, M. R.: Greenland ice sheet climate and surface mass balance in CESM2, Journal of Geophysical Research-Earth Surface, submitted, 2019a.

Van Kampenhout, L., Rhoades, A. M., Herrington, A. R., Zarzycki, C. M., Lenaerts, J. T. M., Sacks, W. J., and van den Broeke, M. R.: Regional grid refinement in an Earth system model: impacts on the simulated Greenland surface mass balance, The Cryosphere, 13, 1547
10   – 1564, https://doi.org/10.5194/tc-13-1547-2019, 2019b.

Van Wessem, J. M., van de Berg, W. J., Noël, B. P. Y., van Meijgaard, E., Amory, C., Birnbaum, G., Jakobs, C. L., Krüger, K., Lenaerts, J. T. M., Lhermitte, S., Ligtenberg, S. R. M., Medley, B., nd K. van Tricht, C. H. R., Trusel, L. D., van Ulft, L. H., Wouters, B., Wuite, J., and van den Broeke, M. R.: Modelling the climate and surface mass balance of polar ice sheets using RACMO2 – Part 2: Antarctica (1979–2016), The Cryosphere, 12, 1479 – 1498, https://doi.org/10.5194/tc-12-1479-2018, 2018.

15   Wouters, B., Bamber, J. L., van den Broeke, M. R., Lenaerts, J. T. M., and Sasgen, I.: Limits in detecting acceleration of ice sheet mass loss due to climate variability, Nature Geoscience, 6, 613 – 616, https://doi.org/10.1038/ngeo1874, 2013.
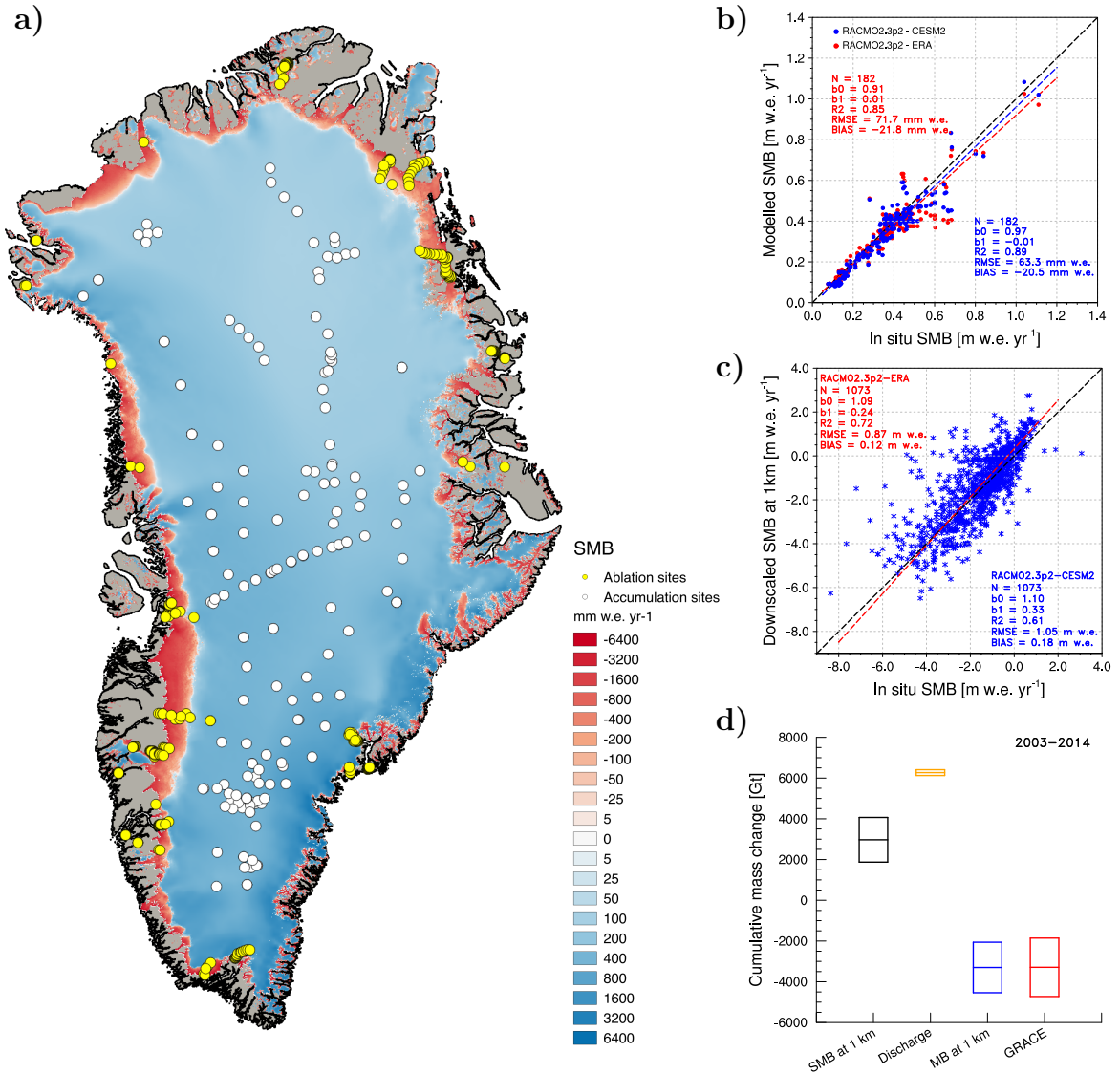
Figure 1. a) Annual mean SMB (1950-2014) as modelled by RACMO2.3p2 forced by CESM2, statistically downscaled to 1 km resolution. b) SMB evaluation in the accumulation zone (182 sites; white dots in Fig. 1 a) and c) in the ablation zone of the GrIS (213 sites; yellow dots in Fig. 1a). Statistics including the number of observations (N), slope (b0) and intercept (b1) of the regressions, determination coefficient (R^2), RMSE and bias are listed for the ERA (red) (Noël et al., 2018) and CESM2-forced RACMO2.3p2 simulation (blue). d) Period (2003-2014) cumulative SMB (black), glacial discharge (orange) (Mouginot et al., 2019), mass balance (MB = SMB - Discharge; blue) and mass loss derived from GRACE (red) (Wouters et al., 2013). To enable a direct comparison with GRACE in d), SMB is integrated over the GrIS, peripheral ice caps and tundra regions of Greenland. Boxes represent one standard deviation around the mean (horizontal bars).
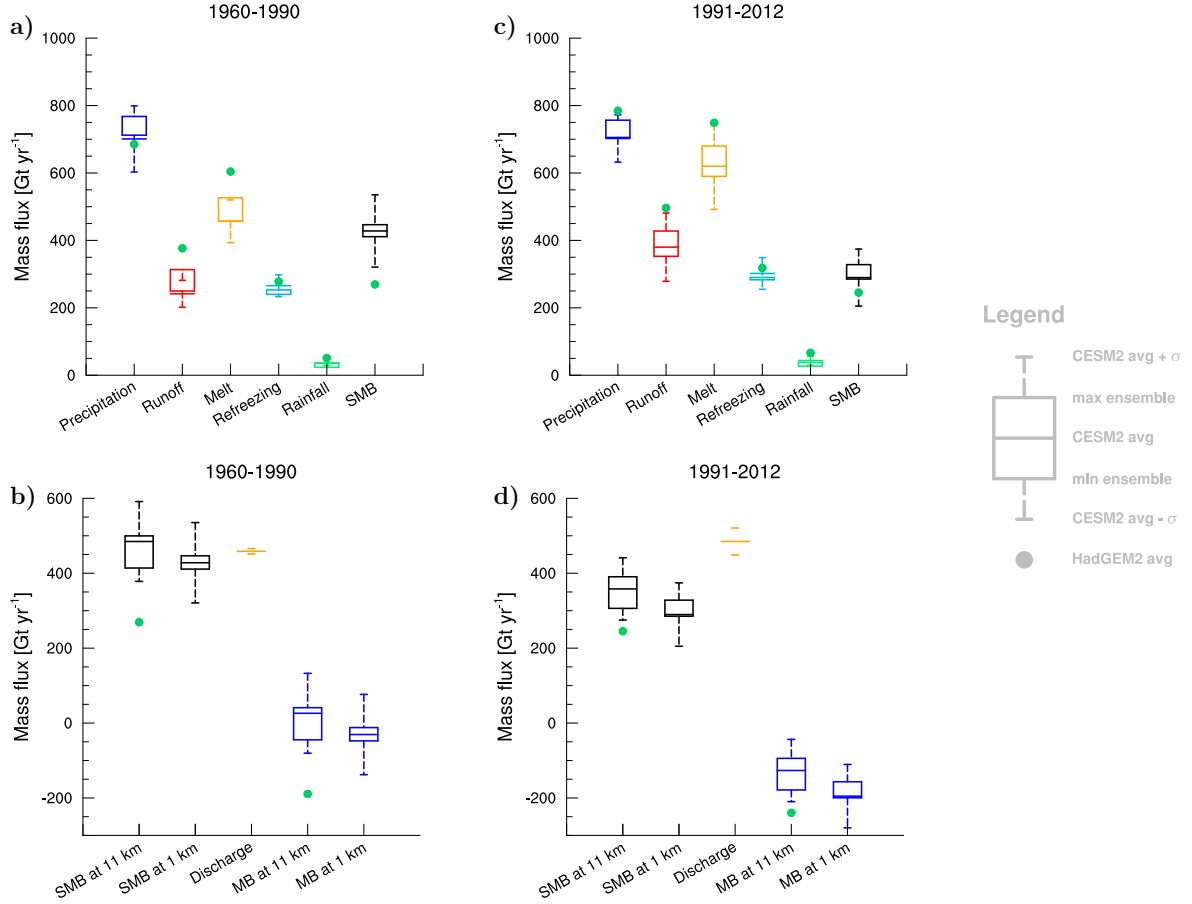
Figure 2. a) Average GrIS SMB (black) and components at 1 km, i.e. total precipitation (blue), runoff (red), melt (orange), refreezing (cyan) and rainfall (green), for the period 1960-1990. b) Annual mean SMB (black), glacial discharge (orange) (Mouginot et al., 2019) and mass balance (MB = SMB - Discharge; blue) at 11 km and 1 km resolution for the period 1960-1990. c) and d) same as a) and b) for the period 1991-2012. The green dots represent values from a previous HadGEM2-forced RACMO2.1 simulation. Boxes around the CESM2-forced RACMO2.3p2 mean (horizontal bars) represent the range of modelled estimates from an ensemble of RACMO2 simulations (five at 11 km, one at 5.5 km, and four at 1 km; Tables A1 and A2). The error bars represent one standard deviation (σ) around the CESM2-forced RACMO2.3p2 mean.

Table A1. Annual mean SMB and components integrated over the GrIS (Gt yr^{-1}) for the period 1960-1990 from an ensemble of RACMO2 simulations using various spatial resolutions and lateral forcing. The uncertainty range corresponds to one standard deviation around the mean. Here mass balance of the GrIS (MB) is estimated as GrIS-integrated SMB minus glacial discharge for the period 1960-1990 (458 Gt yr^{-1}) (Mouginot et al., 2019).

1960-1990	Reference	Forcing	Grid	MB	SMB	PR	RU	ME	RF	RA
RACMO2.1	Van Angelen et al. (2013a)	HadGEM2	11 km	-189±97	269±104	685±82	377±65	604±116	278±66	51±15
RACMO2.1	Van Angelen et al. (2013b)	ERA	11 km	-22±92	437±99	724±77	247±47	424±60	220±27	44±11
RACMO2.3p1	Noël et al. (2015)	ERA	11 km	-45±91	414±98	693±72	237±48	404±62	189±25	22±6
RACMO2.3p2	Noël et al. (2018)	ERA	11 km	28 ±93	487±100	715±73	197±46	345±58	169±20	23±6
RACMO2.3p2	Noël et al. (2019)	ERA	5.5 km	41±96	500 ±104	731±75	197±47	341±59	164±20	23±6
RACMO2.3p2	This study	CESM2	11 km	26±99	485±107	702±98	187±36	332±66	167±35	23±7
RACMO2.3p1	Noël et al. (2016)	ERA	1 km	-48±100	411±108	768±76	313±55	527±66	240±28	24±6
RACMO2.3p2	Noël et al. (2018)	ERA	1 km	-36 ±98	423±106	712±73	257±53	457±56	250±23	35±6
RACMO2.3p2	Noël et al. (2019)	ERA	1 km	-12 ±101	447±109	731±75	250±53	460±59	253±21	33±6
RACMO2.3p2	This study	CESM2	1 km	-31 ±100	428±107	701±98	242±40	457±63	266±32	37±8

Table A2. Annual mean SMB and components integrated over the GrIS (Gt yr^{-1}) for the period 1991-2014 from an ensemble of RACMO2 simulations using various spatial resolutions and lateral forcing. The uncertainty range corresponds to one standard deviation around the mean. Here mass balance of the GrIS (MB) is estimated as GrIS-integrated SMB minus glacial discharge for the period 1991-2012 (485 Gt yr^{-1}) (Mouginot et al., 2019).

| 1991-2012	Reference	Forcing	Grid	MB	SMB	PR	RU	ME	RF	RA
RACMO2.1	Van Angelen et al. (2013a)	HadGEM2	11 km	-240±80	245±141	785±84	496±114	749±156	318±54	67±17
RACMO2.1	Van Angelen et al. (2013b)	ERA	11 km	-155±80	330±116	731±64	361±100	588±146	279±65	52±14
RACMO2.3p1	Noël et al. (2015)	ERA	11 km	-179±83	306±119	685±64	336±99	543±145	233±60	26±8
RACMO2.3p2	Noël et al. (2018)	ERA	11 km	-95±78	389±114	709±61	286±92	470±133	208±53	26±8
RACMO2.3p2	Noël et al. (2019)	ERA	5.5 km	-94±81	391±117	717±62	291±91	469±131	203±53	26±8
RACMO2.3p2	This study	CESM2	11 km	-127±47	358±83	704±70	314±93	495±131	211±51	32±14
RACMO2.3p1	Noël et al. (2016)	ERA	1 km	-200±95	285±131	757±66	428±109	680±146	283±53	27±9
RACMO2.3p2	Noël et al. (2018)	ERA	1 km	-170±85	315±121	705±61	357±101	590±136	28±52	38±8
RACMO2.3p2	Noël et al. (2019)	ERA	1 km	-157±85	328±121	717±63	353±96	594±131	290±50	36±8
RACMO2.3p2	This study	CESM2	1 km	-195±49	290±85	702±70	380±101	620±128	302±47	44±13
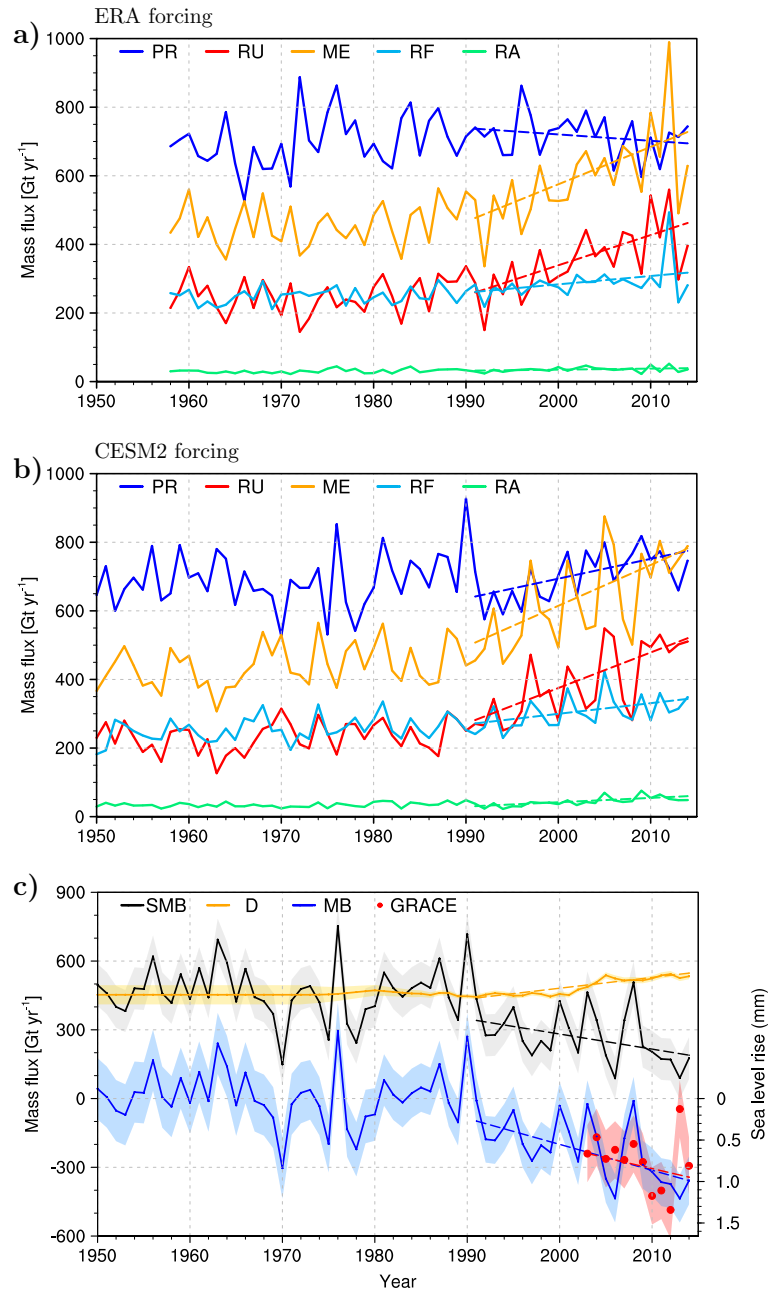
Figure 3. Time series of downscaled (1 km) GrIS-integrated annual SMB components, namely total precipitation (PR; blue), runoff (RU; red), melt (ME; orange), refreezing (RF; cyan) and rainfall (RA; green), as modelled by a) ERA-forced RACMO2.3p2 (1958-2014) (Noël et al., 2019) and b) CESM2-forced RACMO2.3p2 (1950-2014). c) Time series of annual SMB (CESM2-forced RACMO2.3p2 at 1 km), glacial discharge (D) (Mouginot et al., 2019) and mass balance (MB = SMB - D). Mass loss from GRACE (2003-2014) is represented by red dots (Wouters et al., 2013). Dashed lines show the 1991-2014 trends. To enable a direct comparison with GRACE in c), SMB is integrated over the GrIS, peripheral ice caps and surrounding tundra regions of Greenland.
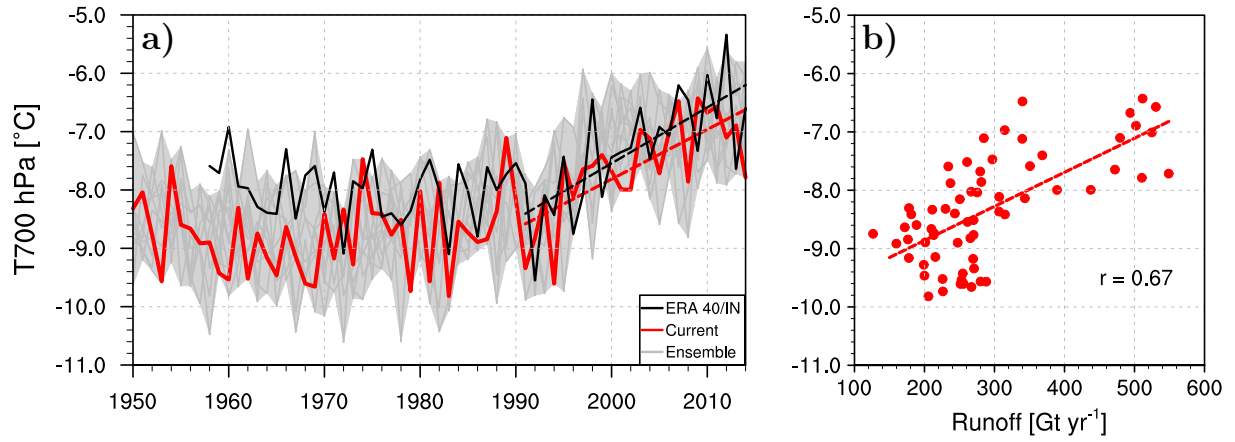
Figure 4. a) Time series of the annual June-July-August (JJA) atmospheric temperature at 700 hPa (T_{700}) averaged over 60-80°N and 20-80°W for the ERA-40 (1958-1978) and ERA-Interim (1979-2014) reanalyses (black), the current CESM2 simulation (red) and 11 additional reference ensemble members (dark grey). The grey belt encompasses annual minimum and maximum values of the whole ensemble. b) Annual GrIS-integrated runoff derived from CESM2-forced RACMO2.3p2 at 1 km resolution as a function of JJA atmospheric temperature at 700 hPa from the current CESM2 simulation (red).